Origin of the Spring-time Westerly Bias in Equatorial Atlantic Surface Winds in CAM3/CCSM3 Model Simulations

Ching-Yee Chang, Sumant Nigam, and *James A. Carton*

Department of Atmospheric and Oceanic Science
University of Maryland, College Park, MD 20742

Submitted to the *Journal of Climate* on July 5, 2007

Corresponding author address: Sumant Nigam, 3419 Computer & Space Sciences Bldg.
University of Maryland, College Park, College Park, MD 20742; Email: nigam@atmos.umd.edu

Abstract

.

The study makes the case that westerly bias in the surface winds of the NCAR atmospheric and coupled models (CAM3 and CCSM3, respectively) over the equatorial Atlantic in boreal spring has its origin in the rainfall (diabatic heating) bias over the tropical South American continent. The case is made by examination of the spatio-temporal evolution of regional precipitation and wind biases, and by dynamical diagnoses of the westerly wind bias from experiments with a steady, linearized dynamical core of an atmospheric general circulation model. Diagnostic modeling indicates that underestimation of rainfall over the eastern Amazon region can lead to the westerly bias in equatorial Atlantic surface winds.

The study suggests that efforts to reduce coupled model biases, especially seasonal ones, must target continental biases, even in the deep Tropics where ocean-atmosphere interaction generally rules.

1. Introduction

Trade winds (easterlies) prevail over most of the tropical Atlantic and Pacific Oceans through the course of the year, being strongest in the northern Tropics in summer. Their seasonal fluctuation has a profound influence on sea surface temperature (SST) in the central and eastern basins; and vice-versa. Along the equator, easterly winds generate equatorial upwelling and cold SST, but not simultaneously across all longitudes: Cold SSTs first appear in the far eastern basin, and their leading edge then moves westward generating a tongue of cold SSTs; the cold-tongue is maximally extended in August-September. The easterlies relax in boreal spring, in conjunction with the deepening of the thermocline and appearance of warm SSTs in the eastern basin.

Simulation of the seasonal cycle of the equatorial trade winds is however challenging for both atmospheric and coupled ocean-atmosphere-land general circulation models (AGCM/ CGCM; Davey et al. 2002; Okumura and Xie 2004; DeWitt 2005; Chang et al. 2007). Davey et al. showed the equatorial zonal wind stress to be too weak in many non-flux-corrected CGCMs. Okumura and Xie (2004) found equatorial westerlies to prevail over the eastern half of the basin in winter and spring in an AGCM. DeWitt (2005) showed the weak zonal wind stress along the equator to be the likely cause of the simulated zonal SST-gradient error. The westerly bias in the Atlantic trade winds is thus a common simulation deficiency, but one whose origin remains unclear.

The present study seeks to investigate the cause of the westerly wind bias, especially, along the equator, in the CAM3 (NCAR's Community Atmosphere Model, version 3; Collins et al. 2006a) and CCSM3 (Community Climate System Model, version 3; Collins et al. 2006b) simulations. The wind bias in these simulations was documented in Chang et al. (2007), who also

examined the bias in related atmospheric and oceanic fields. These authors noted with interest the accompaniment of surface westerly bias by upper-level (200 hPa) easterly bias and deficient (excess) rainfall over Amazon (Africa) in the simulations; that is, a weaker Walker circulation in the Atlantic sector. The westerly bias in surface winds was also linked to the anomalously deep CCSM3 thermocline. Based on bias structures, Chang et al. discuss potential causes of the bias, suggesting deficient rainfall over the Amazon as one possibility.

Local mechanisms have also been proposed to account for the westerly trade wind bias in model simulations. These include insufficient generation of stratus clouds (Yu and Mechoso 1999) and coastal upwelling (Large and Danabasoglu 2006), but whether they are the symptoms or the cause remains to be seen. The notion that deficient Amazonian rainfall can be the ultimate cause of Atlantic sector biases in atmospheric and oceanic fields is an interesting, but heretical one, for two decades of ENSO research has emphasized the primacy of ocean-atmosphere coupling in shaping variability in/over the tropical oceans. Land-atmosphere coupling has however been shown to be important in initiating and setting the pace of seasonal variability over the tropical oceans, the eastern basins in particular; through the timing and location (e.g., coastline orientation) of continental convection; for example, Mitchell and Wallace (1992). The Atlantic basin is, if anything, more susceptible to land influences than the eastern tropical Pacific because of its smaller zonal extent, sandwiched between two major continental convection centers (Amazonia to the west and Africa to the east).

The present study investigates the hypothesis that deficient Amazonian rainfall is the root cause of the westerly bias in equatorial surface winds over the Atlantic. While the hypothesis can be fully tested only with an AGCM, a diagnostic modeling analysis is presented to make the case. The magnitude and extent of the surface wind influence of deficient latent heating over the

Amazon is computed using a steady, linearized dynamical core of an AGCM. The diagnostic model is described in section 2 along with the data sets used in this study. The seasonal evolution of westerly wind, precipitation and diabatic heating biases and related evidence that prompted the hypothesis on the controlling influence of Amazonian convection is presented in section 3. Dynamical diagnosis of CAM3's westerly bias in equatorial Atlantic surface winds, including those establishing the viability of the model, is presented in section 4. Synopsis and concluding remarks follow in section 5, where westerly wind and rainfall biases from a recent CAM development simulation[1] are presented, in support of the case made in this study.

2. Data Sets and Diagnostic Model

a. Simulation data sets

The model simulations analyzed here are the same as in Chang et al. (2007). The mean of a 5-member ensemble of T-85 resolution CAM3 AMIP simulations is analyzed.[2] The CCSM3 simulations come from the "20th Century Climate in Coupled Models" project of the Intergovernmental Panel on Climate Change and are archived at the Program for Climate Model Diagnosis and Intercomparison (PCMDI) website, as case *b30.030a* (20C3M run1). This coupled integration, initiated in 1870, is forced by historical ozone, solar, volcanic, greenhouse gases, and sulfur dioxide/trioxide distributions.

b. Precipitation

Monthly precipitation analysis, based on satellite and gauge measurements, comes from the

[1] The simulation was generated with a CAM development model (CAM3_3_fv_cmt2_dilute) that incorporated improvements to the deep convection scheme (Richter-Neale). These together with cloud-fraction and land model improvements will constitute CAM3.5, whose release is imminent.

[2] These simulations are referred as the "vanilla-AMIP", as they have no external forcing beyond the supplied SST field; as opposed to the "IPCC-AMIP" runs where volcano, greenhouse gases, aerosols, and solar related external forcing are additionally applied.

Global Precipitation Climatology Project (GPCP, version 2; Adler et al. 2003). Data is available on a 2.5° x 2.5° grid over both land and ocean, for the 1979-2006 period.

c. ERA-40 atmospheric analysis

The European Centre for Medium-Range Weather Forecasts (ECMWF) 40-year global reanalysis (ERA-40; Uppala et al 2005) spans September 1957-August 2002 and is locally available on a 2.5° global grid and 23 levels in the vertical. The reanalysis combines model forecast fields, satellite data, radiosonde and other in-situ data, including aircraft and ship reports, with 3D-VAR data assimilation. The ERA-40 assimilating model is the modified ECMWF Integrated Forecasting System which is a T-159 spectral resolution model with 60 vertical levels. The 1979-onward reanalysis, benefiting from inclusion of satellite data, is used in assessing model simulations and in generating the basic state and forcing fields for the diagnostic model.

d. Surface winds

Surface wind speed estimates (combined with wind directions from ECMWF analysis) are available on a 1˚x1˚ longitude-latitude grid for the1988-2000 period from the Special Sensor Microwave Imager (Atlas et al. 1996), and this record is supplemented by the QuikSCAT scatterometer winds (Graf et al. 1998) for the period mid-1999 to 2006.

e. Diagnosed diabatic heating

Diabatic heating was diagnosed in-house using the ERA-40 isobaric reanalyses at 2.5º resolution (Chan and Nigam 2007). Heating was diagnosed as a residual in the thermodynamic equation (e.g., Hoskins et al. 1989; Nigam 1994), using monthly-averaged data and sub-monthly transient fluxes; just as it was earlier for NCEP and ERA-15 reanalyses in Nigam et al. (2000).

f. Diagnostic model

The steady linear primitive equation (SLPE) model solves the σ-coordinate ($\equiv p / p_s$, where p_s is surface pressure) primitive equations. The equations are linearized about a zonally symmetric basic state, and the model solves for the eddy component (i.e., deviation from the zonal average) of the circulation. The linearized model equations are given in the appendix of Held et al. (1989). In order to realistically represent the thermal and momentum diffusion processes in the planetary boundary layer, the simplified Rayleigh momentum dissipation and Newtonian temperature damping terms in these equations are replaced by linearized versions of the vertical momentum and thermal diffusion terms (Nigam 1997). The diffusion coefficients vary in the boundary layer, decreasing rapidly above 925 hPa. The inclusion of diffusive mixing leads to lower boundary conditions on zonal and meridional velocity, and temperature, requiring specification of drag coefficients, CDU, CDV, and CDT. In addition to vertical diffusive mixing in the planetary boundary layer, the thermodynamic and horizontal momentum equations include horizontal diffusive mixing, with a constant coefficient of $1 \times 10^6 m^2 s^{-1}$. Additional model details can be found in the appendix of Nigam (1994) and Nigam and Chung (2000). All model parameters are specified exactly as in Nigam (1997), except for the drag coefficients CDU and CDV, which are both set equal to 1.0×10^{-3} instead of 1.5×10^{-3}.

The diagnostic model is solved numerically, using the semi-spectral representation for horizontal structure: 73 grid points between the two poles ($\Delta\theta = 2.5°$), and zonal Fourier truncation at wavenumber 30 (equivalent to $\Delta\lambda = 6.0°$), where θ is latitude and λ the longitude. The vertical structure is discretized using 18 full-sigma levels of which 14 are in the troposphere, including 5 below 850 hPa. The semi-spectral model was preferred in view of strong latitudinal

variation of tropical features, such as the Inter-Tropical Convergence Zone.

3. CAM3 Biases in the Tropical Atlantic

a. Westerly wind bias

The seasonal evolution of surface zonal wind at the equator is shown in the upper panels of Fig. 1 at monthly resolution.[3] Both satellite based wind observations and ERA-40 reanalysis capture the seasonal cycle – annual in the western and semi-annual in the eastern basin – quite well. Model simulations fare well in the latter half of the calendar year, but not in boreal spring when westerlies are present in most basin longitudes, and not just the eastern sector (as in observations). The westerly bias in modeled surface winds is extensively documented in Chang et al. (2007), who show the entire deep Tropics (10°S-10°N) to be biased, with the zonal-wind bias peaking at the equator; see their Fig. 4. The westerly bias is evidently amplified in the presence of an interactive ocean, for CCSM3's bias is twice as large, and a bit delayed, as well. The westerly bias effectively changes the character of seasonal variability in the eastern basin, from semi-annual to annual, especially in the CCSM3 simulation.

An intercomparison of observed and modeled zonal wind evolution (upper panels in Fig. 1), especially, the slope of westerly wind contours in the winter-to-spring months, initially suggested an eastern origin of the bias, tempering efforts to connect the bias (and the weaker Walker circulation) with Amazonian rainfall. Plotting the bias itself, however, clarified the situation: The CAM3 bias with respect to ERA-40 (lower middle panel in Fig. 1) clearly shows the westerlies to originate in the western sector, e.g., from tracking of the +2 m/s contour.

[3] The 20-year simulation climatologies are only marginally different from the 50-year climatologies shown in Chang et al. (2007).

b. Precipitation bias

The precipitation bias structure provides further insight into the origin of the westerly bias. CAM3's bias in Amazonian and African precipitation with respect to GPCP rainfall is shown in the lower left and right panels of Fig. 1, respectively; with the panel lineup in accord with regional geography. Immediately apparent is the big deficit in eastern Amazon rainfall (by 6-7 mm/day) and its timing. The maximum deficit is in March, i.e., during the peak of the local rainy season. Interestingly, the deficit develops near-synchronously with the westerly bias, which peaks in March-April; the wind-bias lags Amazon rainfall by, at most, a month. CAM3's bias relative to ERA-40 rainfall (not shown) is very similar. The spatio-temporal structure of the eastern Amazon rainfall deficit and the downstream westerly wind bias thus provide strong, albeit circumstantial, evidence for an Amazonian origin of the Atlantic Walker circulation bias in CAM3/CCSM3 simulations.

Connection of the westerly bias with simulation errors in African rainfall – the other anchor point of the Atlantic Walker circulation – is examined in the lower right panel of Fig. 1. Unlike over the Amazon, CAM3 generates excessive rainfall over much of Africa. The year-round excess is, typically, 3-4 mm/day except in summer when it is lower. Evolution of the westerly bias in the *eastern* basin indicates some susceptibility to the African rainfall errors. Diagnostic modeling analysis, discussed later, however shows the Amazon influence to dominate over most of the Atlantic basin.

The off-equatorial distribution of observed and simulated precipitation over the Amazon and surrounding regions (land and ocean) is displayed in Fig. 2 (left panels), for the peak westerly-bias period, March-May. The CAM3 bias shows rainfall over tropical South America to

be deficient, especially, over the eastern Amazon (−5 mm/day) and Andes (−2 mm/day); in both cases, the deficiency is as large as ~50% of the local climatology, and thus quite significant. The rainfall deficits are reflected in the diabatic heating distribution, shown next.

c. Diabatic heating bias

Diabatic heating, generated from both cloud-scale and large-scale processes, is the principal forcing of the tropical circulation. The latent heating component is dominant in the deep Tropics, especially in regions of deep convection, such as the Inter-Tropical Convergence Zone, the Western Pacific Warm Pool, and the Amazon. A close correspondence between precipitation and vertically averaged diabatic heating is expected in these regions, and this expectation is borne out in Fig. 2 (right panels). The correspondence is particularly striking in the middle panels, where both fields are from CAM3. Note the similar location of the field maxima. The correspondence in the top panels is not as striking since the fields are from different sources and because residual diagnosis of heating in regions of steep orography is more uncertain, especially if the underlying circulation and temperature analyses are not well anchored by observations; the case over most of South America. Even so, the correspondence over eastern Amazon is notable and manifest in the similarity of this region's heating and precipitation biases.

4. Dynamical Diagnosis of CAM3's Westerly Bias in Surface Winds

Modeling analysis that provides insight into the origin of CAM3's westerly bias over the equatorial Atlantic is reported here. The dynamical diagnosis is conducted using a diagnostic model – a choice that needs some justification in view of vigorous ocean-atmosphere-land interaction in the Tropics. As noted before, the westerly bias is present in both CAM3 and CCSM3 simulations, albeit more robustly in the latter, indicating that this bias is not rooted in

ocean-atmosphere interactions. The same however cannot be said for land-atmosphere interactions since rainfall generation and distribution is governed by a number of processes including those dependent on the land-surface state. The use of an atmosphere-only diagnostic model, as here, can thus be limiting, especially if the analysis goals extend beyond identification of geographic regions exerting unrealistic local and remote influences. The present analysis seeks only such identification in context of CAM3's Atlantic sector biases, deferring further analysis of the causes of aberrant model behaviour over the South American continent to a later study.

A prerequisite for dynamical diagnosis is the diagnostic model's ability to simulate the target field: the CAM3's Atlantic sector bias, here. If notable features of the bias can be simulated, its origin can be investigated, at least, in a diagnostic (*a posteriori*) sense. For a meaningful analysis, the model should be required to simulate the individual circulations (observed, CAM3) as well.[4] This assessment is made in Fig. 3 which shows the observed and diagnostically simulated March-May surface circulations after removal of the zonal-mean component; i.e., only the eddy components are shown. The zonal-mean component is removed as the diagnostic model is linearized about it; making this circulation component common to the target and simulated fields.

a. Model assessment: March-May simulation

In the Fig. 3 simulation, the zonal-mean zonal and meridional velocities, temperature, and surface pressure from ERA-40 are the 2D model inputs (basic state specification); and orography, surface temperature, and diagnosed 3D diabatic heating and submonthly transient heat and momentum fluxes are the model forcing. The surface circulation, consisting of sea-level pressure

[4] Or better yet, their average. The bias (a−b) and average (a+b) are independent states, and a model that simulates both offers prospects for a more insightful analysis.

(SLP) and 1000 hPa winds, is of direct interest in view of the westerly surface wind bias; both target (ERA-40) and simulated surface fields are shown. The SLP-high in the tropical/subtropical Atlantic (and Pacific) is reasonably simulated, except for the amplitude; the mid-latitude simulation is even better. In the Tropics, where SLP is no longer a proxy for the winds, the simulated trade winds are weak in the northern, but not southern, tropical Atlantic. The reasonable simulation of ERA-40's March-May surface circulation clears the way for the next level of model assessment: its potential in simulating the CAM3 bias.

b. Model assessment: Bias simulation

The simulated CAM3 bias is shown in Fig. 4, with target fields in the top panel. The simulation is obtained without transient forcing, mechanical or thermal; and as the difference of two diagnostic model solutions: One obtained with ERA-40 zonal-mean basic state, surface temperature, orography, and diagnosed 3D diabatic heating, while the other with the CAM3 counterparts. The thermal and mechanical transient forcing is not applied in each case, in part, because the sub-monthly transient fluxes were unavailable in the CAM3 archive. Note, the zonally-asymmetric component of the SLP and 1000 hPa winds are displayed in both cases.

The bias simulation is reasonable, but not as remarkable as the simulation of the ERA-40 surface circulation (cf. Fig. 3); in part, because of the missing impact of transient fluxes, which can be significant, especially outside of the deep Tropics. CAM3's westerly bias in the equatorial Atlantic is, nonetheless, captured, albeit with weaker amplitude; just as in Fig. 3. The westerly bias cannot all be attributed to heating differences in view of other model-input differences (orography, surface temperature and zonal-mean basic state). The latter differences are eliminated in the following section through the use of ERA-40 fields in both cases.

c. Diagnosis of CAM3's equatorial westerly bias

The geographic region whose heating contributes most to the equatorial westerly bias in the Atlantic is identified in this section from diagnostic modeling experiments in which heating-bias in selected regions is used as model forcing; all other fields are from ERA-40. The modeled circulation bias can then be unambiguously attributed to the select region's heating bias.

The surface circulation forced by the global tropical (15ºS to 15ºN) heating bias is shown in Fig. 5a. Almost all of the SLP bias (~ 1 hPa) and westerly wind bias (~ 3 m/s) in the western equatorial Atlantic originates in the Tropics, not surprisingly. Note the smaller (half) SLP contour interval in Fig. 5. In the interest of space, only the surface simulation is displayed. The influence of regional heating biases in the Tropics is examined next, beginning with the South American sector (80ºW-35ºW, 10ºS-12.5ºN; marked rectangle in panel *b*). Panel comparisons indicate that between half-to-two-thirds of the westerly bias attributed to the Tropics (panel *a*) originates in the South American region. The sector's influence is far from local, extending up to the African shores. The maximum westerly response, ~1.6 $\mathrm{m\,s^{-1}}$, is located ~30ºW, i.e., close to the location of CAM3's peak westerly bias. The structure of the surface response, with westerlies to the east of the eastern Amazon cooling (cf. Fig. 3) and easterlies to its west, indicates weaker surface convergence and ascending motion over the eastern Amazon in CAM3.

The next two panels parse the Fig. 5b response into parts forced by the land and ocean sector heating biases. The surface circulation forced by the continental heating bias is shown in panel *c*. Its structure is similar to the total response (panel *b*) but the amplitude is smaller, being one-third to half of the latter: The continental forced westerly bias is ~0.6 m/s at 30ºW, i.e., significant; especially, since continental convection biases are less labile than oceanic ones, in

part, because the land-surface state (e.g., soil moisture) cannot change as readily as SST can from equatorial and coastal upwelling. Efforts to reduce coupled model biases, especially seasonal ones, must target the biases in continental regions. A large body of work on seasonal cycle variability in the eastern tropical Pacific (beginning with Mitchell and Wallace's 1992 study) would also argue for such a strategy.

The CAM3 simulation differs from ERA-40 not only in the horizontal distribution of vertically averaged diabatic heating (and thus precipitation in the Tropics), but also in its vertical structure. The heating profiles for the South American region are shown in Fig. 6, separately for the land and ocean sectors. The CAM3 profile is quite distinct from ERA-40's, particularly, over land where it is weaker (stronger) in the mid (lower) troposphere. The excessive low-level heating in CAM3 results from strong sensible heating, arising from warmer than observed land surface temperature (not shown). The CAM3 difference from ERA-40, also plotted, is, interestingly, a mirror image of the heating profile typically associated with stratiform convection (cf. Houze 1997); reflecting, potentially, under-simulation of stratiform rainfall in CAM3.

The heating profile is very influential in the deep Tropics, as latent heating is largely offset by ascent induced adiabatic cooling there, resulting in the pressure vertical velocity (ω) mimicking the heating profile ($N^2\omega \approx Q$, where N^2 is static stability and Q the diabatic heating rate). The heating vertical structure is thus directly tied to the divergent circulation through the continuity equation, and to the rotational flow via the stretching term of the vorticity equation. It is thus of some interest to examine if the heating amount or heating profile differences are more consequential in context of CAM3's westerly bias.

The influence of heating profile differences is assessed by computing the model's response to synthetic heating distributions. These are obtained from multiplication of the vertically averaged heating field by the regionally averaged heating profile, resulting in each grid point of the region having the same heating vertical structure. The synthetic distributions are assessed in Fig. 5d, which shows the model response forced by the heating bias over tropical South America, just as in panel *c*, except for the use of synthetic CAM3 and ERA-40 heating. The close similarity of surface circulations in panel *c* and *d* attests to the viability of this analysis strategy in ascertaining the role of profile differences in generation of CAM3's westerly wind bias over the equatorial Atlantic.

The influence of the South American land heating bias is shown in Fig. 7, with the amount and profile effects separated out. In the top panel, CAM3's heating was modified to have the same profile as ERA-40 heating, while still retaining the amount bias. The resulting surface response shows that the westerly bias attributed to heating bias over tropical South America (cf. Figs. 5 c-d) arises largely from heating amount rather than profile differences. The impact of the profile bias on surface circulation (Fig. 7b) was found to be significant as well, but confined to the continental forcing region. The heating profile bias over tropical South America evidently contributes little to the Atlantic westerly bias.

It is interesting to note the opposite sign of the South American SLP response generated by the amount and profile biases in Fig. 7. The positive SLP in the former case arises from reduced latent heating amount (in mid-troposphere), with concomitant reduction in offsetting ascent, and thus low-level convergence, all consistent with a positive SLP response. The negative SLP response in the profile case arises from excessive low-level heating (and mid-troposphere cooling) in CAM3 (cf. left panel in Fig. 6), whose compensation requires ascent and low-level

convergence in the near surface levels; thus, a negative SLP signal.[5]

5. Concluding Remarks

The study makes the case that westerly bias in CAM3's surface winds over the equatorial Atlantic in boreal spring, and indeed, also in the corresponding coupled model's (CCSM3) surface winds, has its origin in the rainfall (diabatic heating) bias over the tropical South American continent. The case is made from examination of the spatio-temporal evolution of regional precipitation and wind biases, and from dynamical diagnoses of the westerly wind bias from experiments with a steady, linearized dynamical core of an atmospheric general circulation model. Diagnostic modeling indicates that underestimation of rainfall over the eastern Amazon region can lead to westerly bias in equatorial Atlantic surface winds.

A continental origin for a key coupled model bias in the deep Tropics seems somewhat far-fetched at first in view of vigorous ocean-atmosphere interaction in equatorial regions; as, for example, during El Nino Southern Oscillation variability. Implicating deficient modeling of land-atmosphere interaction (leading to diminished continental convection and rainfall) as the source of the downstream westerly bias however seems more reasonable upon further reflection, especially in view of the large body of work on seasonal variability in the eastern tropical Pacific, beginning with Mitchell and Wallace (1992). Their analysis showed continental convection to be the pace maker in seasonal climate evolution in the eastern tropical basins. [Seasonal variability in these regions is pronouncedly annual despite incident insolation being dominantly semi-annual.]

[5] By the same token, sinking and horizontally divergent flow must occur in the mid troposphere, with higher pressure there. From a column perspective, oppositely-signed circulations occur at different levels, but these mass-balanced flows provide limited insight into the hydrostatic basis for the resulting SLP response.

Important support for the South American origin of the Atlantic westerly wind bias comes from a recent CAM development simulation (see footnote 1 for more details). The simulation was produced at NCAR in early 2007 using a CAM3 version that included improvements to the deep convection scheme. [The improved scheme (Richter-Neale) will be standard in the soon-to-be-released CAM3.5 model.] The westerly bias in the equatorial Atlantic and rainfall bias in the tropical American-Atlantic-African sector are displayed in Fig. 8. Immediately apparent is the significant reduction in the westerly wind bias, by more than 1 m/s (cf. Fig. 1). Also notably diminished is the rainfall bias over the eastern Amazon (and Andean region); but not the ITCZ/rainfall bias over the tropical Atlantic, which is only marginally weaker. The new bias structures support the claim for a defining role of eastern Amazon rainfall deficiencies in generation of the westerly bias in equatorial Atlantic surface winds.

Our analysis would be incomplete without addressing the role of African rainfall bias in generation of the westerly bias over the equatorial Atlantic. The African bias is broadly of the opposite sign and about half as large as the eastern Amazon bias, especially, in the CAM development simulation; biases of both signs are present along the coast in CAM3. If the African bias was influential, a larger westerly wind bias should be in evidence in the development simulation in view of the coherent and stronger positive rainfall bias in this case. This is however not the case, for the westerly bias is found to be notably diminished in this simulation (cf. Fig. 8). Diagnostic modeling also shows the influence of the African rainfall (diabatic heating) bias to be largely confined to the far eastern basin; supporting the assessment of a limited role of African rainfall bias in generation of the westerly bias in the western/central equatorial Atlantic basin.

Finally, it is of some interest to inquire about the fate of the westerly bias in a coupled ocean-atmosphere environment. The bias is larger in CCSM3 (cf. Fig. 1), as noted before,

indicating the lack of any corrective/negative feedbacks in this coupled model. Chang et al. (2007) argue that westerly bias leads to deeper thermocline (and warmer SSTs) in the eastern equatorial basin, with the SST-gradient change generating additional westerlies (cf. Lindzen and Nigam 1987); that is, for the existence of a positive feedback, which amplifies the bias.

Acknowledgements

The authors would like to thank Steven C. Chan for providing access to the diabatic heating field diagnosed from ERA-40 reanalysis, in advance of publication of the related paper; Alfredo Ruiz-Barradas and Renu R. Joseph for help in acquiring the CAM3 and CCSM3 datasets; and Semyon A. Grodsky and Jin-Ho Yoon for helpful discussions.

References

Adler, R.F., et al., 2003**:** The Version-2 Global Precipitation Climatology Project (GPCP) Monthly Precipitation Analysis (1979–Present). *J. Hydrometeorology*, **4**, 1147–1167.

Atlas, R., R. Hoffman, S. Bloom, J. Jusem, and J. Ardizzone, 1996: A multi-year global surface wind velocity data set using SSM/I wind observations. *Bull. Amer. Meteor. Soc.*, **77**, 869-882.

Chan, S., and S. Nigam, 2007: Intercomparison of diabatic heating diagnosed from ERA-40, ERA-15, and NCEP-NCAR reanalyses (To be submitted to *J. Climate*, August 2007).

Chang, C.-Y., J. A. Carton, S. A. Grodsky, and S. Nigam, 2007: Seasonal climate of the tropical Atlantic sector in the NCAR Community Climate System Model 3: Error structure and probable causes of errors. *J. Climate*, **20**, 1053-1070.

Collins, W. D., C. M. Bitz, M. L. Blackmon, G. B. Bonan, C. S. Bretherton, J. A. Carton, P. Chang, S. C. Doney, J. J. Hack, T. B. Henderson, J. T. Kiehl, W. G. Large, D. S. McKenna, B. D. Santer, and R. D. Smith, 2006a: The Community Climate System Model Version 3 (CCSM3). *J. Climate*, **19**, 2122-2143.

Collins, W. D., P. J. Rasch, B. A. Boville, J. J. Hack, J. R. McCaa, D. L. Williamson, B. P. Briegleb, C. M. Bitz, S-J. Lin, and M. Zhang, 2006b: The formulation and atmospheric simulation of the Community Atmosphere Model Version 3 (CAM3). *J. Climate*, **19**, 2144-2161.

Davey, M., M. Huddleston, K.R. Sperber et al., 2002: STOIC: A study of coupled model climatology and variability in tropical ocean regions. *Clim. Dyn.*, **18**, 403-420.

DeWitt, D. G., 2005: Diagnosis of the tropical Atlantic near-equatorial SST bias in a directly coupled atmosphere-ocean general circulation model. *Geophys. Res. Lett.*, **32**, L01703, doi:10.1029/2004GL021707

Graf, J., C. Sasaki, C. Winn, W.T. Liu, W. Tsai, M. Freilich, and D. Long, 1998: NASA

Scatterometer Experiment. *Acta Astronautica*, **43**, 397-407.

Held, I. M., S.W. Lyons, and S. Nigam, 1989: Transients and the extratropical response to El Niño. *J. Atmos. Sci.*, **46**, 163-174.

Hoskins, B. J., H. H. Hsu, I. N. James, M. Masutani, P. D. Sardeshmukh, and G. H. White, 1989: Diagnostics of the global atmospheric circulation based on ECMWF analyses 1979-1989. *WCRP-27; WMO/TD-No. 326*, 217pp.

Houze, R. A., Jr., 1997: Stratiform precipitation in regions of convection: A meteorological Paradox? *Bull. Amer. Meteor. Soc.,* **78**, 2179-2196.

Large, W.G. and G. Danabasoglu, 2006: Attribution and impacts of upper-ocean biases in CCSM3. *J. Climate*, **19**, 2325-2346.

Lindzen, R.S., and S. Nigam, 1987: On the role of sea surface temperature gradients in forcing low-level winds and convergence in the tropics. *J. Atmos. Sci.*, **44**, 2418-2436.

Mitchell, T. P., and J. M. Wallace, 1992: The annual cycle in equatorial convection and sea surface temperature. *J. Climate,* **5**, 1140–1156.

Nigam, S., 1994: On the dynamical basis for the Asian summer monsoon rainfall-EL Nino relationship. *J. Climate*, **7**, 1750-1771.

Nigam, S., and Y. Chao, 1996: Evolution dynamics of tropical ocean–atmosphere annual cycle variability. *J. Climate,* **9**, 3187–3205.

Nigam, S., 1997: The annual warm to cold phase transition in the eastern equatorial Pacific**:** Diagnosis of the role of stratus cloud-top cooling. *J. Climate*, **10**, 2447-2467.

Nigam, S., C. Chung, and E. DeWeaver, 2000: ENSO diabatic heating in ECMWF and NCEP Reanalyses, and NCAR CCM3 simulation. *J. Climate,* **13**, 3152-3171.

Nigam, S., and C. Chung, 2000: ENSO surface winds in CCM3 simulation: diagnosis of errors. *J. Climate*, **13**, 3172-3186.

Okumura, Y., and S.-P. Xie, 2004: Interaction of the Atlantic Equatorial Cold Tongue and the African Monsoon. *J. Climate,* **17**, 3589-3602.

Uppala, S. M., and Coauthors, 2005: The ERA40 reanalysis. *Q. J. Royal Met. Soc.*, **131**, 2961-3012.

Yu, J.-Y., and C. R. Mechoso, 1999: A discussion on the errors in the surface heat fluxes simulated by a coupled GCM. *J. Climate,* **12,** 416–426.

Figure Captions

Figure 1: Seasonal evolution of the surface zonal wind (upper panels, 1 m/s), zonal wind bias (lower middle, 1 m/s), and rainfall bias in the equatorial American and African sectors (lower left and right panels, respectively, 1 mm/day). Data is averaged over 2^{o}S-2^{o}N in all panels. Wind is from the 1000 hPa level in model simulations. The GPCP rainfall climatology is for the 1979-2005 period.

Figure 2: Precipitation (left, 1 mm/day) and diabatic heating (right, 0.5 K/day) distribution over tropical South America in observations and CAM3 simulation during March-May. Observationally derived fields are in the top panels, CAM3 ones in the middle, and the CAM3 bias (e.g., CAM3−ERA-40) in the bottom panels. The mass-weighted vertical average (175 hPa to the surface) of heating is displayed. The marked rectangle in the bottom panels indicates the tropical region whose influence is subsequently investigated.

Figure 3: Observed and diagnostically simulated March-May surface circulation (zonally asymmetric part) in the Pacific and Atlantic sectors: Sea-level pressure and 1000 hPa winds from ERA-40 reanalysis are shown in the upper panel, while their simulation from the SLPE model is shown in the lower panel, using the same contour interval and vector scale. The SLPE model is forced by orography, 3D diabatic heating, and submonthly thermal and vorticity transient fluxes, all obtained/diagnosed from the ERA-40 reanalysis. Wind vectors are not plotted when the wind speed is less than 1 m/s, and values over land are masked out

prior to computation of the zonally-asymmetric component.

Figure 4: CAM3's surface circulation *bias* (upper panel) and its diagnostic simulation (lower panel): The zonally asymmetric part of sea-level pressure and 1000 hPa winds is shown, as in Fig. 3. The diagnostic simulation is obtained without thermal and mechanical transient forcing bias. The SLP contour interval and wind vector scale are indicated in the title line. Positive SLP bias is shaded red.

Figure 5: Diagnostic analysis of CAM3's March-May surface circulation *bias*: From (a) global tropical (15ºS-15ºN) heating bias; (b) tropical South American (marked box) heating bias; (c) tropical South American *continental* heating bias; and (d) synthetic continental heating bias. The latter is obtained by multiplication of vertically averaged heating by the average heating profile over tropical South American land. SLP contour interval (half of Fig. 4) and wind vector scale are indicated in the title line. Vector scale in the top panel is twice as large as in the rest. Bias vectors of less than 0.2 m/s wind speed are not plotted. Positive SLP bias is shaded red.

Figure 6: Diabatic heating profiles over the tropical South American region: Average profile over the continental (oceanic) region of the box marked in Fig. 5 is displayed in the left (right) panels. Both observationally constrained (ERA-40 residual diagnosis, blue) and CAM3 simulated (red) profiles are shown, along with the CAM3 bias (green).

Figure 7: Diagnostic analysis of CAM3's March-May surface circulation *bias* (contd.): Bias

forced by synthetic heating over the tropical South American continent (land in the marked box), consisting of only the (a) CAM3 heating *amount* bias, and (b) CAM3 heating *profile*. bias. Rest as in Fig. 5.

Figure 8: Surface zonal wind (left panel) and tropical precipitation (right) biases in a CAM3 development simulation (Richter-Neale deep convection, see footnote 1 for more details). CAM3's precipitation bias in an expanded tropical sector is also shown to facilitate comparison. Rest as in Fig. 1.

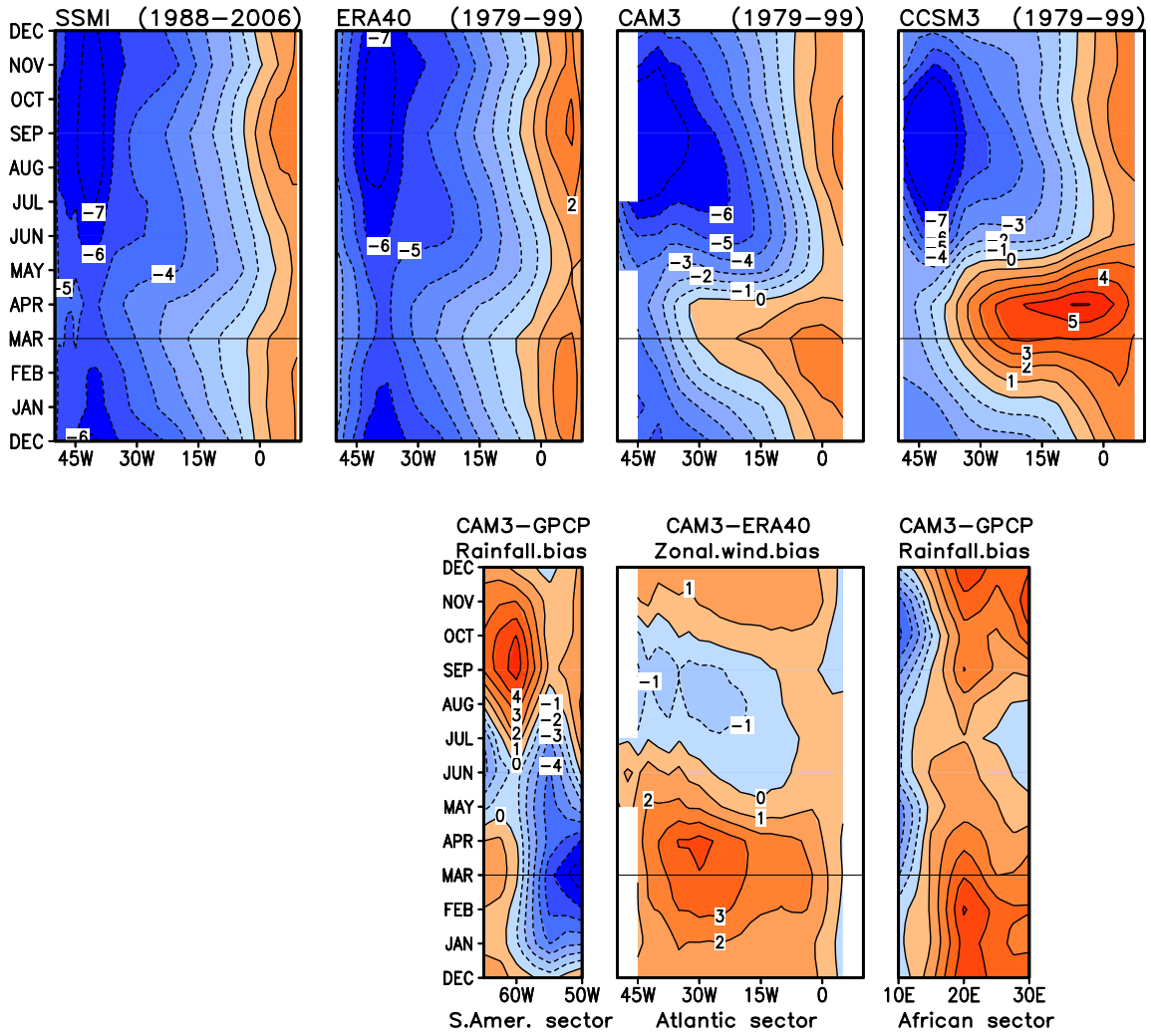

Figure 1: Seasonal evolution of the surface zonal wind (upper panels, 1 m/s), zonal wind bias (lower middle, 1 m/s), and rainfall bias in the equatorial American and African sectors (lower left and right panels, respectively, 1 mm/day). Data is averaged over 2°S-2°N in all panels. Wind is from the 1000 hPa level in model simulations. The GPCP rainfall climatology is for the 1979-2005 period.

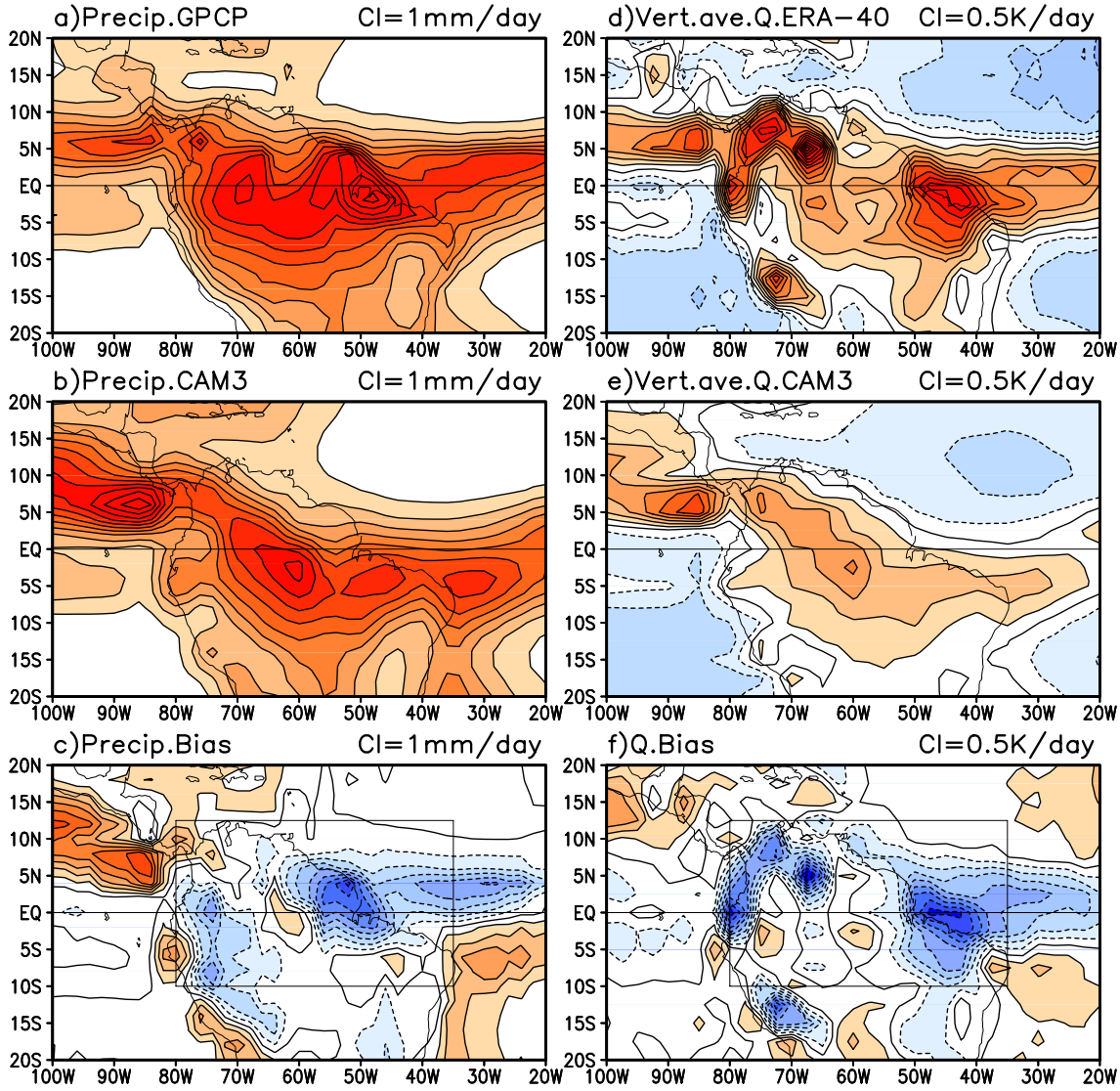

Figure 2: Precipitation (left, 1 mm/day) and diabatic heating (right, 0.5 K/day) distribution over tropical South America in observations and CAM3 simulation during March-May. Observationally derived fields are in the top panels, CAM3 ones in the middle, and the CAM3 bias (e.g., CAM3−ERA-40) in the bottom panels. The mass-weighted vertical average (175 hPa to the surface) of heating is displayed. The marked rectangle in the bottom panels indicates the tropical region whose influence is subsequently investigated.

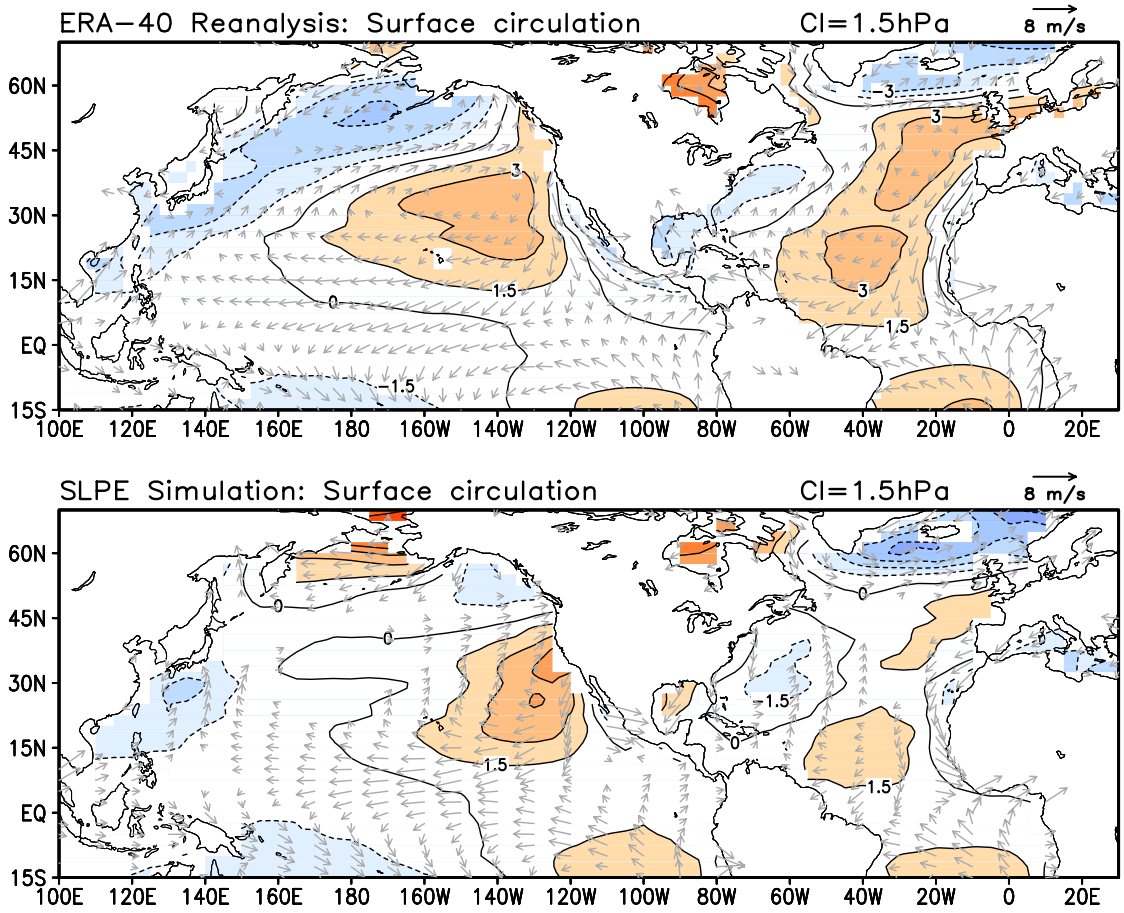

Figure 3: Observed and diagnostically simulated March-May surface circulation (zonally asymmetric part) in the Pacific and Atlantic sectors: Sea-level pressure and 1000 hPa winds from ERA-40 reanalysis are shown in the upper panel, while their simulation from the SLPE model is shown in the lower panel, using the same contour interval and vector scale. The SLPE model is forced by orography, 3D diabatic heating, and submonthly thermal and vorticity transient fluxes, all obtained/diagnosed from the ERA-40 reanalysis. Wind vectors are not plotted when the wind speed is less than 1 m/s, and values over land are masked out prior to computation of the zonally-asymmetric component.

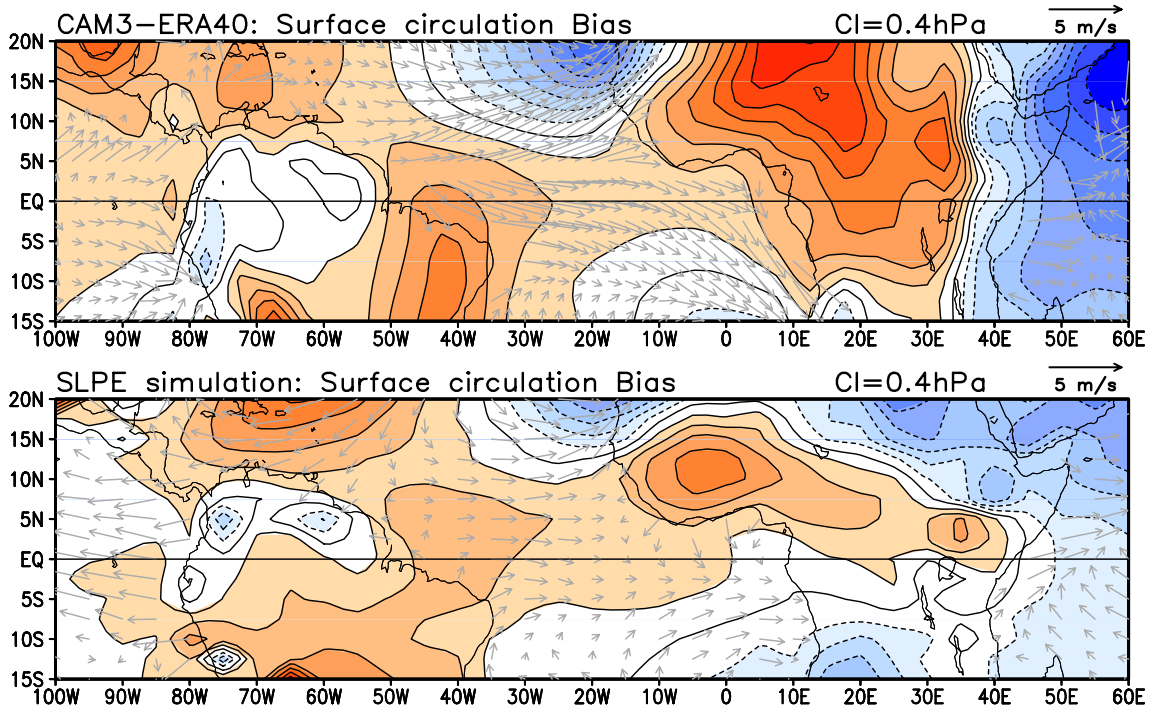

Figure 4: CAM3's surface circulation *bias* (upper panel) and its diagnostic simulation (lower panel): The zonally asymmetric part of sea-level pressure and 1000 hPa winds is shown, as in Fig. 3. The diagnostic simulation is obtained without thermal and mechanical transient forcing bias. The SLP contour interval and wind vector scale are indicated in the title line. Positive SLP bias is shaded red.

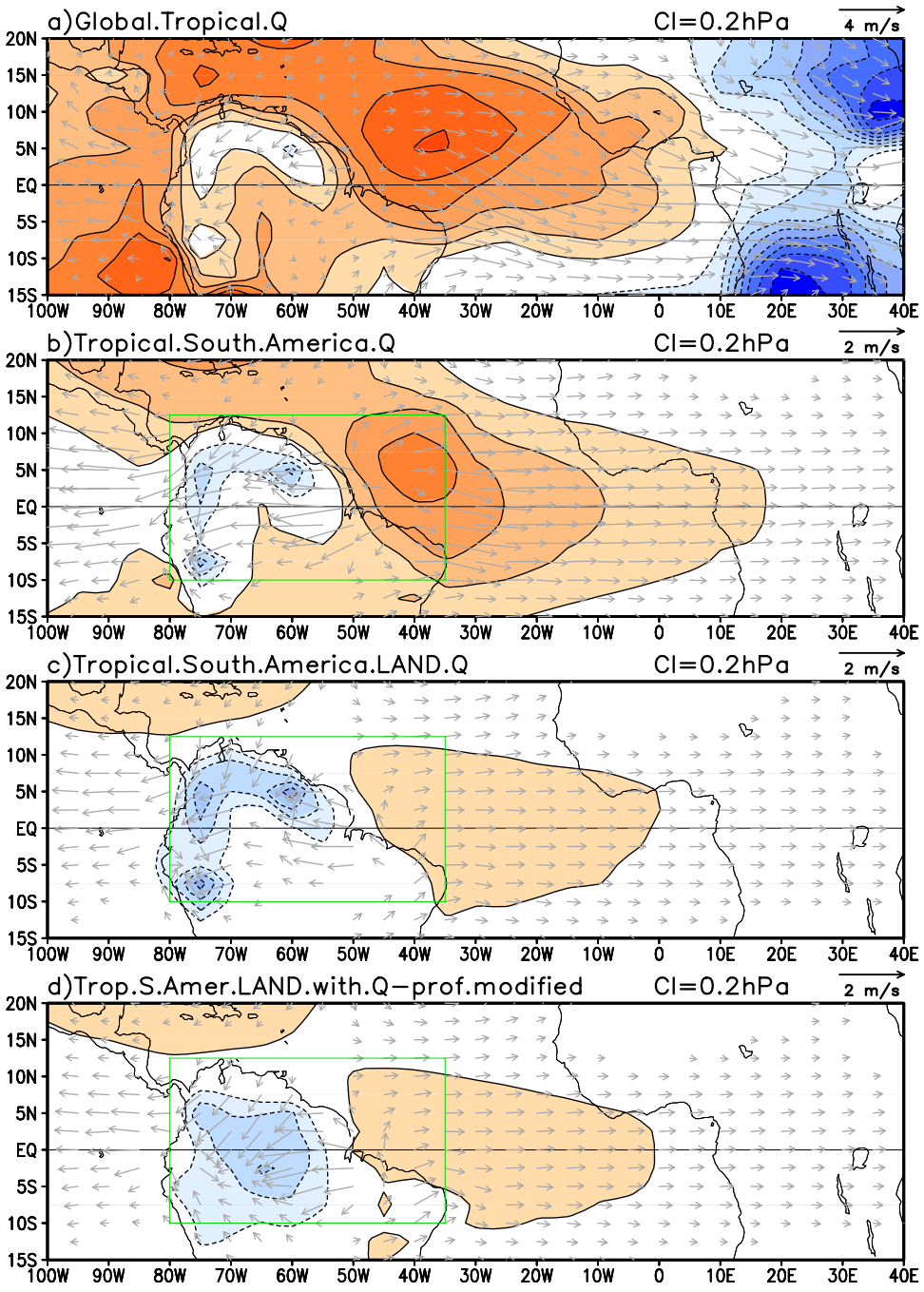

Figure 5: Diagnostic analysis of CAM3's March-May surface circulation *bias*: From (a) global tropical (15ºS-15ºN) heating bias; (b) tropical South American (marked box) heating bias; (c) tropical South American *continental* heating bias; and (d) synthetic continental heating bias. The latter is obtained by multiplication of vertically averaged heating by the average heating profile over tropical South American land. SLP contour interval (half of Fig. 4) and wind vector scale are indicated in the title line. Vector scale in the top panel is twice as large as in the rest. Bias vectors of less than 0.2 m/s wind speed are not plotted. Positive SLP bias is shaded red.

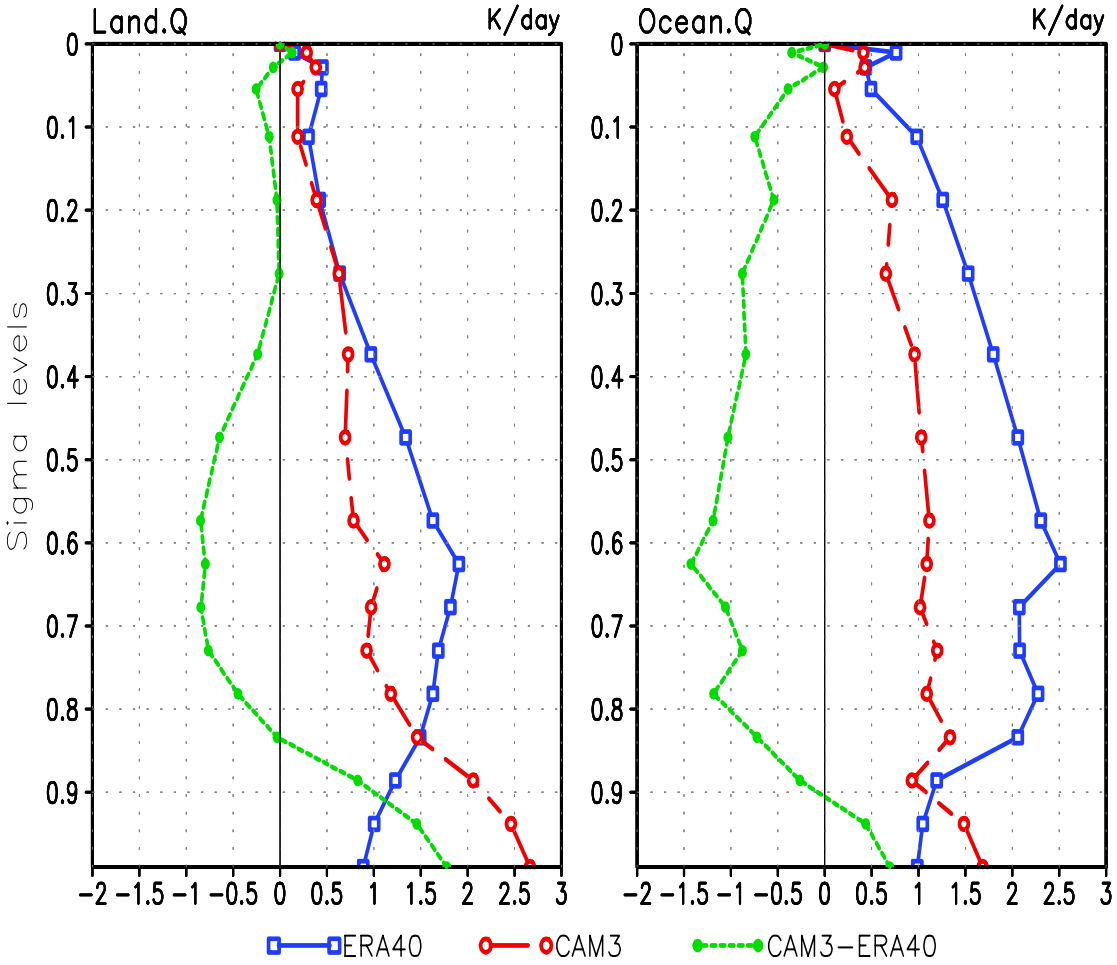

Figure 6: Diabatic heating profiles over the tropical South American region: Average profile over the continental (oceanic) region of the box marked in Fig. 5 is displayed in the left (right) panels. Both observationally constrained (ERA-40 residual diagnosis, blue) and CAM3 simulated (red) profiles are shown, along with the CAM3 bias (green).

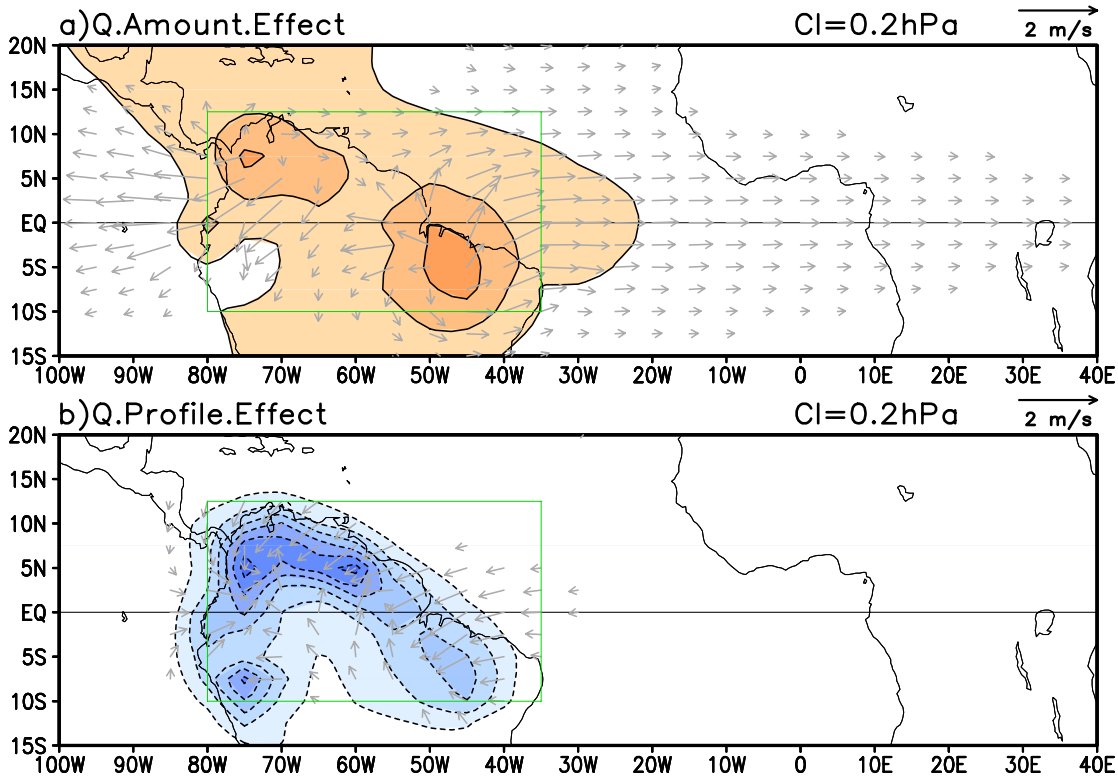

Figure 7: Diagnostic analysis of CAM3's March-May surface circulation *bias* (contd.): Bias forced by synthetic heating over the tropical South American continent (land in the marked box), consisting of only the (a) CAM3 heating *amount* bias, and (b) CAM3 heating *profile*. bias. Rest as in Fig. 5.

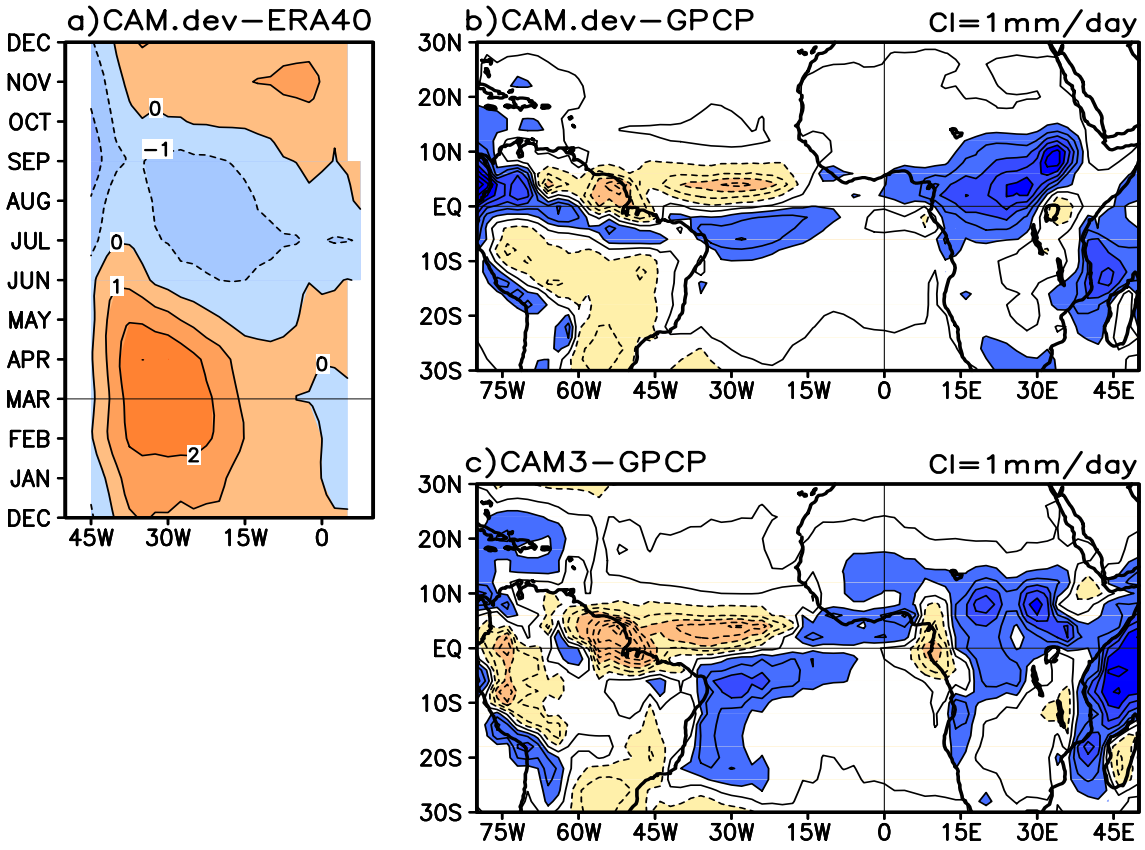

Figure 8: Equatorial surface zonal wind (left panel) and tropical precipitation (right) biases in a CAM3 development simulation (Richter-Neale deep convection, see footnote 1 for more details). CAM3's precipitation bias in an expanded tropical sector is also shown to facilitate comparison. Rest as in Fig. 1.